Medicinal Chemistry

Research Article Open Access

Novel Chiral Chalcone Analogs that Induce M Phase Arrest and Apoptosis in HeLa Cells

Weiwei Chen[1], Ruirong Yi[1], Majid Vahed[1], Yoshifumi Ohno[1], Zheng Tian[1], Shuhan Guo[1], Xue Ma[1], Nan Nwe Win[1], Qisen Li[1], Ayumu Tsubosaka[1], Kengo Saito[1], Shingo Nakamoto[1], Akiko Suganami[1,2,3], Yutaka Tamura[2,3], Takayoshi Arai[4] and Hiroshi Shirasawa[1]*

[1]Department of Molecular Virology, Graduate School of Medicine, Chiba University, 1-8-1 Inohana, Chuo-ku, Chiba 260-8670, Japan
[2]Department of Bioinformatics, Graduate School of Medicine, Chiba University, 1-8-1 Inohana, Chuo-ku, Chiba 260-8670, Japan
[3]Molecular Chirality Research Center, Chiba University, 1-33 Yayoi-chou, Inage-Ku, Chiba 263-8522, Japan
[4]Department of Chemistry, Graduate School of Sciences, Chiba University, 1-33 Yayoi-chou, Inage-Ku, Chiba 263-8522, Japan

Abstract

We identified two chiral chalcone analogs CCL360 and CCL361 from the Chiba Chemical Library, which exhibit antiproliferative effects on human cancer cells. Flow cytometry analyses revealed that HeLa and Vero cells treated with CCL360 and CCL361 had higher populations of cells in the G_2/M phase than untreated cells. Docking studies suggested that the R-isomer of CCL361 binds to the taxol binding domain (TBD) of β-tubulin, and the S-isomers of CCL360 and CCL361 bind to β-tubulin at the colchicine binding domain and the TBD. Further investigations using a fluorescent ubiquitination-based cell cycle indicator system revealed that the two compounds caused cell cycle arrest (in the M phase) and apoptosis only in HeLa cells. In non-cancerous Vero cells, however, CCL360 and CCL361 prolonged the G_2/M phase without causing apoptosis. Although increased expression levels of p53 and p21 were observed in all CCL360/361-treated cells, only HeLa cells exhibited increased levels of cleaved poly (ADP-ribose) polymerases and apoptosis. Increases in G_2/M phase populations in CCL360/361-treated cells are likely caused by increases in p-histone H3 (at Ser10) and Cyclin B1 levels. Furthermore, CCL360/361-treated HeLa cells exhibited phosphorylation of p-Plk1 (at Thr210) and dephosphorylation of p-Cdc2 (at Tyr15); these changes were not evident in CCL360/361-treated Vero cells, suggesting that the link between p53 and Plk1 in HeLa cells was likely compromised. Our study indicates that CCL360 and CCL361 are microtubule-targeting agents that can be used as lead compounds for developing novel anticancer drugs.

Keywords: Cell cycle; M phase arrest; HeLa; Vero; Chalcone analog; Anticancer compound

Introduction

Globally, cancer is one of the leading causes of death [1]. Cancer treatment often involves chemotherapy, which aims to reduce cancer cell growth with one or more anticancer drugs in standardized regimens. Microtubule-targeting agents (MTAs) are commonly used anticancer drugs that interfere with microtubule dynamics [2-5].

Microtubules, which are composed of α- and β-tubulin heterodimers, play essential roles in various cellular processes, including cell division, cell migration, and intracellular transportation [6]. In the eukaryotic cell cycle, microtubules aid in the segregation of the daughter chromosomes during cell division [3,7]. As microtubule dynamics are essential for cell division, they have been an attractive target for cancer therapy. MTAs interfere with microtubule dynamics and arrest cancer cells in the G_2/M phases; this can eventually induce apoptosis in cancer cells [8-10].

As MTAs disturb microtubule dynamics, these drugs often work by blocking the cell's entry into mitosis; a checkpoint regulates this entry at the boundary between the G_2 and M phases of the cell cycle [11]. Activation of cyclin B–Cdc2 (also known as Cdk1) is an essential molecular event required for the initiation of mitosis [12-15]. Cyclin B–Cdc2 complexes are activated by dephosphorylation of Cdc2 at Thr14 and Tyr15 (both of which are phosphorylated by the protein kinases Wee1 and Myt1) by the protein phosphatase Cdc25C. Cdc25C is phosphorylated and activated by Polo-like kinase 1 (Plk1), which in turn, is activated by phosphorylation at a conserved residue (Thr210) in its T loop [15-18]. Mitosis is tightly regulated at the spindle assembly checkpoint (SAC) to ensure proper chromosomal segregation [19,20]. MTAs activate the SAC, which sustains the Cdc2 activation, inhibiting the degradation of cyclin B1 that controls the time to mitotic exit [20].

The MTAs in current use as anticancer agents can be categorized into two classes: (a) ligands that inhibit the formation of the microtubule (such as colchicine) and (b) compounds that inhibit the disassembly of the microtubule (such as taxol) [21]. Chalcones, which are naturally occurring intermediates of flavonoid compounds, have earned great interest as potential anticancer agents exhibiting colchicine-type activity [21]. The core structure of chalcones has two aromatic rings connected by a three-carbon α,β-unsaturated carbonyl bridge [22]. Thus, it is worthwhile to evaluate whether chalcone analogs, which exhibit chirality, work as MTAs. In this study, we investigated the anticancer activity and underlying mechanisms of action of two novel chalcone analogs, CCL360 and CCL361, which were identified by screening the Chiba Chemical Library (CCL) for anticancer drugs.

Materials and Methods

Chemical compounds

(Z)-2-(hydroxy(4-methoxyphenyl)methyl)-3-methyl-1-phenylhex-2-en-1-one (CCL360) and (Z)-2-(hydroxy(p-tolyl)methyl)-3-methyl-1-phenylhex-2-en-1-one (CCL361) were identified by

***Corresponding author:** Hiroshi Shirasawa, Department of Molecular Virology, Graduate School of Medicine, Chiba University, 1-8-1 Inohana, Chuo-ku, Chiba 260-8670, Japan, Tel: +81-43-226-2044; Fax: +81-43-226-2045; E-mail: sirasawa@faculty.chiba-u.jp

Received September 16, 2019; **Accepted** September 24, 2019; **Published** September 30, 2019

Citation: Chen W, Yi R, Vahed M, Ohno Y, Tian Z, et al. (2019) Novel Chiral Chalcone Analogs that Induce M Phase Arrest and Apoptosis in HeLa Cells. Med Chem (Los Angeles) 9: 74-82.

screening the CCL and were manufactured in our laboratory. Stock solutions (20 mM) of CCL360 and CCL361 were prepared in dimethyl sulfoxide (DMSO, Wako).

Cell lines

HeLa cells were obtained from the American Type Culture Collection (ATCC). Vero cells were cultured from the laboratory stock [23]. Cells were grown in Dulbecco's modified Eagle's medium (DMEM, Sigma-Aldrich) with 10% fetal bovine serum (FBS, Thermo Fisher Scientific) at 37 °C in 5% CO_2. The HeLa-FUCCI and Vero-FUCCI cell lines were established using a previously described protocol [24].

Determination of cell viability

Cells were seeded in 96-well plates at densities of 2×10^3 cells/well. After 24 h of culture, the cells were treated with increasing concentrations of CCL360 or CCL361 and incubated for 24 h. Control cells were exposed to volumes of DMSO equivalent to those of CCL360 or CCL361 solutions that were added to the treated cells. Cell viability was determined using the CellTiter-Glo® Luminescent Cell Viability Assay (Promega). The luminescent signal was measured using a Wallac 1420 Multilabel counter (PerkinElmer). Data are presented as proportions of viable cells (in %) by comparing the CCL360/361-treated cells with the DMSO-treated cells (considered to have a viability of 100%).

Staining and imaging of cultured cells

Following CCL360/361 treatment, cells were stained with Hoechst 33342 (Thermo Fisher Scientific) and incubated for 5 min at 37°C. Cells were then imaged with a UV-2A filter (excitation wavelength 365 nm, emission wavelength 400 nm) using the Nikon Eclipse TE2000-U microscope. The fluorescent ubiquitination-based cell cycle indicator (FUCCI) system was used to visualize the cell cycle behavior of individual cells treated with CCL360 or CCL361. To image HeLa-FUCCI and Vero-FUCCI cells, 4×10^4 cells were grown overnight in a 35 mm dish (Ibidi) in DMEM with 10% FBS at 37°C in 5% CO_2. Following this, cells were exposed to 50 μM CCL360 or CCL361 and subjected to time-lapse imaging using a computer-assisted fluorescence microscope (FV10i, Olympus) at 37 °C in 5% CO_2. Images were recorded every 30 min. Two filter cubes were chosen for fluorescence imaging: mKusabira-orange (excitation wavelength 548 nm, emission wavelength 559 nm) was used to observe FUCCI orange and Azami-Green (excitation wavelength 493 nm, emission wavelength 505 nm) was used to observe FUCCI green. Olympus Fluoview software (version 4.2) was used for image acquisition and analysis.

Western blot analysis

CCL360/361-treated and control cells were collected and washed twice with phosphate-buffered saline (PBS), following which they were resuspended in M-PER® Mammalian Protein Extraction Reagent (Thermo Fisher Scientific) with a cocktail of protease inhibitors (Sigma-Aldrich) and mixed gently for 10 min. Lysates were centrifuged at 14,000 × g for 10 min. Equal amounts of extracted proteins were loaded onto SDS-polyacrylamide gels (Atto Corporation), transferred onto PVDF membranes (Trans-Blot Turbo™ Transfer Pack, BIO-RAD), and labeled with antibodies. Antibodies against p-histone H3 (at Ser10), Cyclin B1, p-Cdc2 (at Tyr15), p-Plk1, p21, poly (ADP-ribose) polymerase (PARP), and β-actin were obtained from Cell Signaling Technology, Inc. Antibodies against p53 were obtained from Santa Cruz Biotechnology, Inc.

Flow cytometry analysis

CCL360/361-treated and control cells were collected and washed twice with PBS, following which, the cells were treated with reagents from the CycleTEST™ PLUS DNA Reagent Kit (Becton Dickinson, USA) and analyzed on a BD Accuri™ C6 Flow Cytometer (Becton Dickinson, USA) equipped with a FACScan fluorescence 2 (FL2) detector. The collected data were analyzed using FlowJo (version 7.6.5, TreeStar, Inc.).

Molecular docking simulations

The atomic coordinates for tubulin were obtained from the cryo-electron microscopy structure of the protein available in the RCSB protein data bank with the accession code 5syf [25]. Before proceeding with the analysis, all water molecules and solvent molecules were removed from the structure. The α- and β-tubulin structures in the αβ-tubulin complex were separated from each other and stored in two separate files for individual docking analyses. The 3-D chemical structures of colchicine, taxol, CCL360, and CCL361 (for both, S and R isomers) were designed using the software Avogadro (version 1.1.1) [26]; the structures were optimized in Gaussian 16 (Gaussian Inc.) at the B3LYP/6-31G (d, p) theoretical level [27,28].

The software AutoDock 4.2 [29] was utilized for molecular docking simulations. Structure files for proteins and ligands were prepared in the PDBQT format using default charges; furthermore, nonpolar hydrogen atoms were merged onto their respective heavy atoms using AutoDockTools (version 1.5.6). A grid box (XYZ dimensions: 76 Å × 76 Å × 76 Å) was centered on the tubulin structure. A pre-calculated binding affinity value for each ligand's atom type was prepared using Autogrid. Rigid docking was carried out using Lamarckian genetic algorithm parameters [30]. All other parameters in the AutoDock 4.2 software were maintained in their default settings. The best pose for docking was selected based on the lowest values of binding energies obtained.

The free binding energies (FBE) and van der Waals (VDW) interactions were calculated using a linear regression model inbuilt in AutoDock 4.2. The hydrophobic surface of β-tubulin was visualized in PyMOL using the Eisenberg hydrophobicity scale [31]. The electrostatic potential of the β-tubulin surface was calculated using the PDB2PQ [32,33] server and the APBS plugin (version 2.1) in PyMOL [32]. The hydrogen bond (H-bond) occupancy for visualization of docked conformations was obtained using PyMOL. The root mean square deviation (RMSD) values for conformational diversity of compounds from the output file of the docking analyses were calculated along with reference structures of ligands (with the dock's input file) using PyMOL. The structure of β-tubulin with helix axes was generated using the molecular modeling software Chimera [33].

Statistical analysis

All values are expressed as mean ± SD (standard deviation) for cytotoxicity assays and flow cytometry analyses or mean ± SE (standard errors) for FUCCI analyses. Statistical analyses were performed using the software Statcel4 (version 4 (OMS)). Values of $P<0.05$ indicated statistical significance.

Results

Cytotoxicities of CCL360 and CCL361 against HeLa and Vero cells

We screened a chemical compound library (CCL) for anticancer compounds that could show selective cytotoxicity against cancerous cell lines; we identified two novel compounds, CCL360, and CCL361 (Figure 1), that exhibited such activity. The cytotoxicities of different

concentrations of CCL360 and CCL361 against HeLa and Vero cells after 48 h of treatment were evaluated using the CellTiter-Glo Luminescent Cell Viability Assay (Figure 2). Both compounds exhibited cytotoxicity in a dose-dependent manner with IC_{50} values (at 48 h) of 43.1 μM (for CCL360) and 36.1 μM (for CCL361) in HeLa cells. The IC_{50} values at the same time point for Vero cells were 97.2 μM (for CCL360) and 70.8 μM (for CCL361). The IC_{50} values of both compounds for Vero cells were approximately 2-fold higher than those for HeLa cells. All further experiments involving these compounds were performed at a concentration of 50 μM.

Effect of CCL360 and CCL361 on the morphologies of HeLa and Vero cells

Treatment with 50 μM CCL360 or CCL361 caused pronounced changes in HeLa cell morphology, such as cell shrinkage, pyknosis, and nuclear condensation (Figure 3); morphological changes in Vero cells were less pronounced, especially those involving nuclear morphology (Figure 3). Hoechst 33342 staining of HeLa cells treated with CCL360/61 for 24 h revealed many cells with broken/fragmented nuclei.

Flow cytometry analysis of HeLa and Vero cells treated with CCL360 and CCL361

To assess the effects of CCL360 and CCL361 on the cell cycle, we treated HeLa and Vero cells with 50 μM CCL360 or CCL361 for 24 h which were analyzed by flow cytometry (Figure 4A). As shown in Fig. 4A, when HeLa and Vero cells were treated with CCL360 or CCL361, the population of cells in G_2/M phases increased. Although the increase

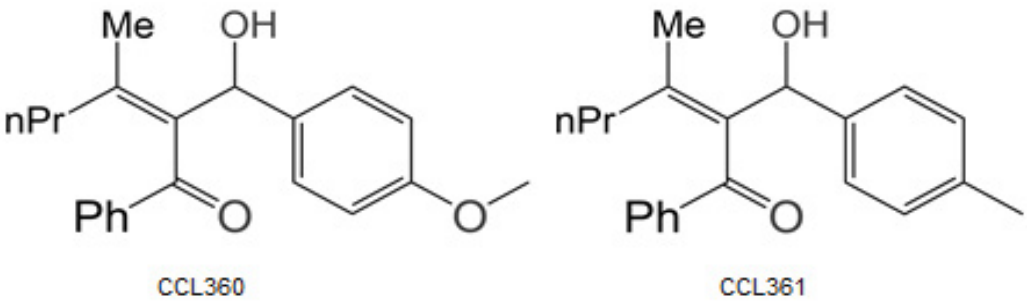

Figure 1: Chemical structures of CCL360 and CCL361. The chemical structures of CCL360 and CCL361 molecules as modeled using the software Avogadro.

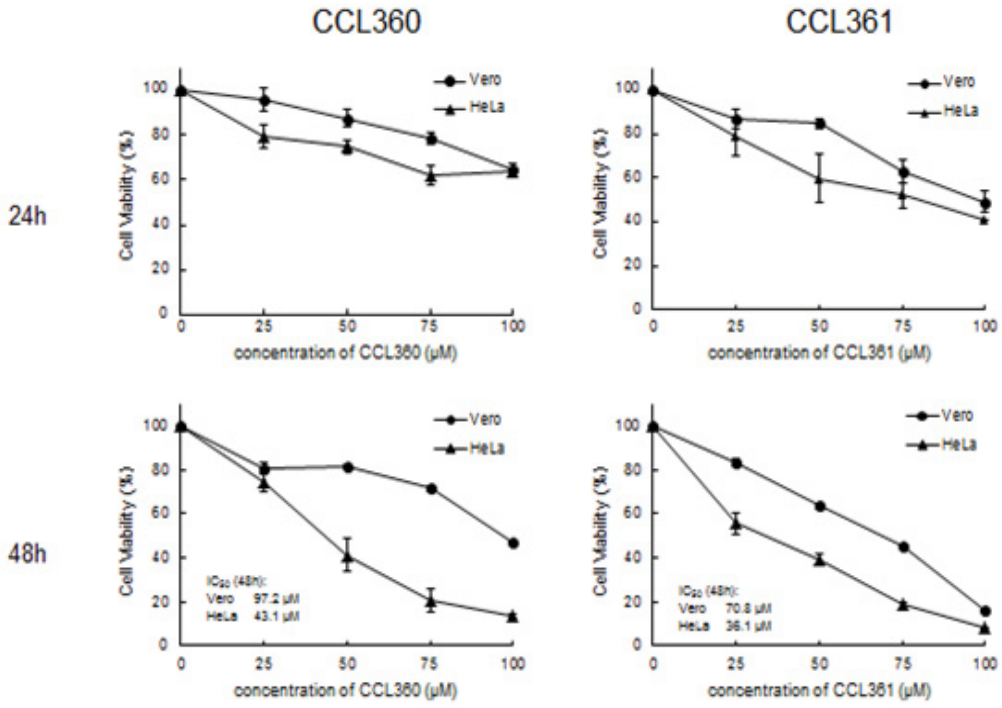

Figure 2: Cytotoxicities of CCL360 and CCL361 against HeLa and Vero cells**.** HeLa and Vero cells were treated with increasing concentrations of CCL360 or CCL361 for 24 and 48 h, following which cell viability was measured using the CellTiter-Glo® Luminescent Cell Viability Assay. Data are shown as mean SD, and cell viabilities are represented as percentages of the control group for three independent experiments.'

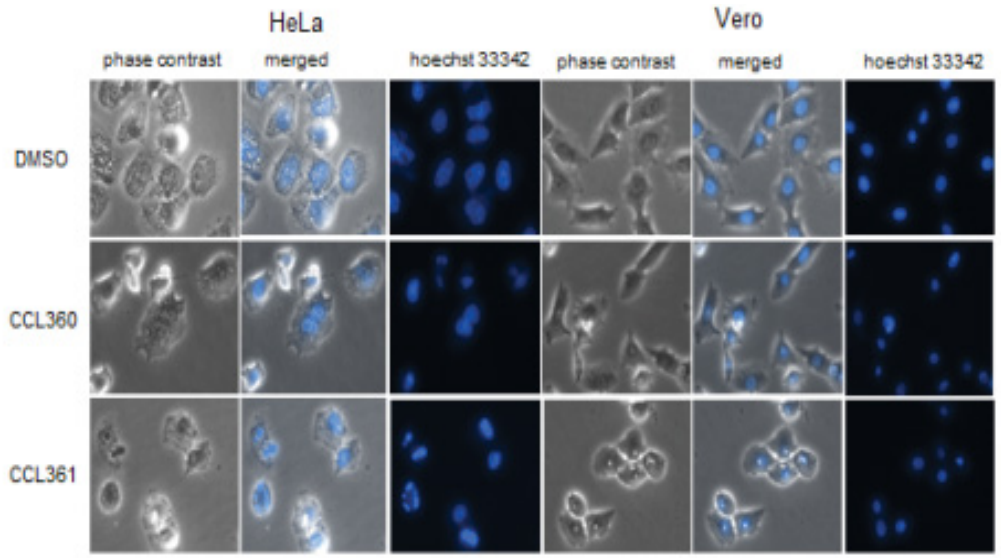

Figure 3: Effect of CCL360 and CCL361 on the morphologies of HeLa and Vero cells. Cells were treated with 50 μM CCL360 or CCL361 for 24 h; control cells were treated with equal volumes of DMSO. The leftmost panel shows phase contrast images, the middle panel shows DNA stained with Hoechst 33342, and the rightmost panel shows merged images in HeLa and Vero cells.

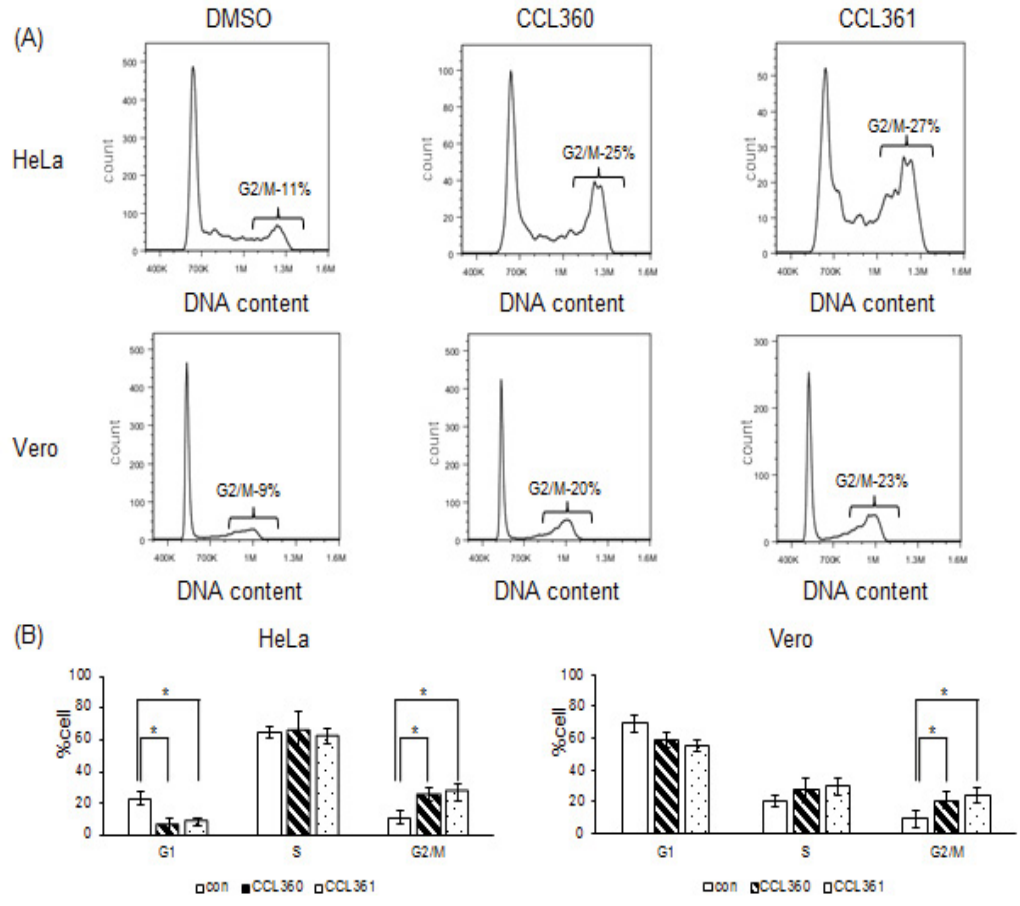

Figure 4: Effects of CCL360 and CCL361 on cell cycle progression. (A) Representative histograms of the flow cytometry data on cell cycle progression in HeLa and Vero cells following 24 h of treatment with 50 μM CCL360, 50 μM CCL361, or DMSO (control). (B)The proportions of HeLa and Vero cells in G_1, S, and G_2/M phases following treatment with DMSO (con), 50 μM CCL360, or 50 μM CCL361. Data are represented as mean ± SD of three independent experiments performed in triplicate plates. *P < 0.05 (Mann-Whitney U-test).

in the populations of G_2/M phase cells was significant ($P < 0.05$) in both cell lines, a significant concomitant reduction in the population of G_1 phase cells was observed ($P < 0.05$) only in the HeLa cell line (Figure 4B). These results suggested that CCL360 and CCL361 induced cell death only in HeLa cells, although both compounds induced G_2/M cell cycle arrest at the G_2/M phase in both HeLa and Vero cell lines.

Interaction of CCL360 and CCL361 with β-tubulin

CCL360 and CCL361 are chalcone analogs; we have demonstrated that both compounds can induce G_2/M arrest in human cell lines. Since some chalcones inhibit the polymerization of tubulin by binding to the colchicine binding domain (CBD) [34], we performed docking analyses to investigate whether the tested compounds also bind to tubulin via the CBD.

Optimal 3-D structures of ligands (CCL360 and CCL361) were generated using the software Gaussian 16 (Figure 5). We also used AutoDockTools to identify energy scores of ligand-protein binding in six complexes between tubulin and CCL360R, CCL360S, CCL361R, CCL361S, colchicine, and taxol. The docking results showed different binding energies for α- and β-tubulin. Since all binding energies were significantly lower for β-tubulin, we opted to use β-tubulin for further ligand-binding analyses.

The FBE affinities of CCL361R to β-tubulin were significantly stronger than those of other ligands (Table 1). Although CCL360 and CCL361 have similar structures, they exhibited different binding properties at the binding sites on the β-tubulin structure (Figure 6A). CCL360R and CCL361R exhibited high binding affinities to the taxol binding domain (TBD), whereas CCL360S and CCL361S exhibited interactions with both, the TBD as well as the CBD of β-tubulin at energy levels of -3 kcal or less. As shown in Table 1, the lowest docking

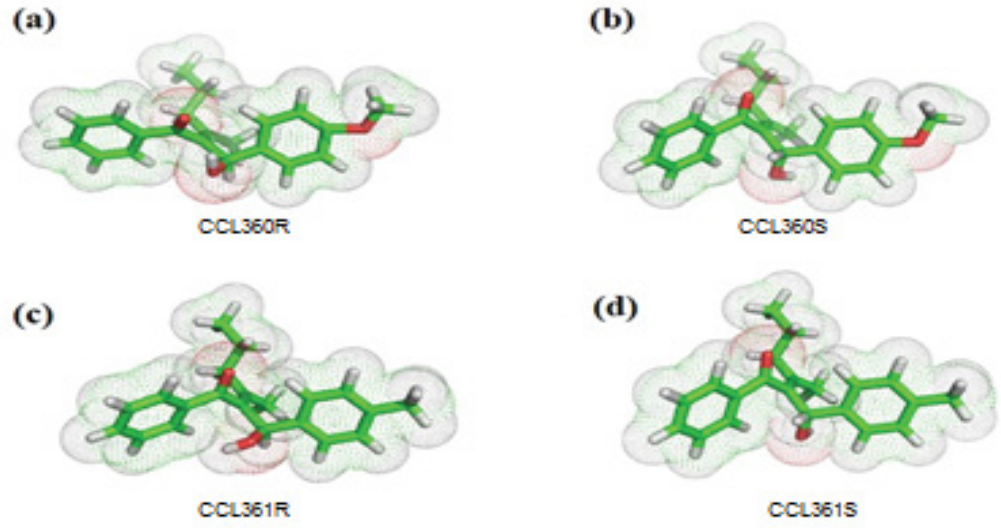

Figure 5: 3-D structures with optimized geometries of CCL360 and CCL361 as created using the software Gaussian 16. (A) CCL360R, (B) CCL360S, (C) CCL361R, (D) CCL361S

FBE Ranking	Docking scores	CCL360R	CCL360S	CCL361R	CCL361S	Colchicine	Taxol
1	FBE*	-2.68	-3.58	-10.82	-3.5	-4.24	-4.81
	VDW**	-5.1	-5.91	1.92	-5.41	-5.63	-9.01
	RMSD***	2.61	2.476	2	2.37	0.36	2.18
	H-bond†	0	1	TBD	1	4	2
	Binding Domain	TBD‡	CBD††		TBD	CBD	TBD
2	FBE	-2.08	-3.42	-3.66	-3.12	-3.94	-3.87
	VDW	-4.25	-5.76	-5.74	-5.19	-5.43	-8.04
	RMSD	2.1	2.83	2.33	2.68	1.09	2.74
	H-bond	1	3	0	0	2	2
	Binding Domain	TBD	TBD	TBD	CBD	CBD	TBD
3	FBE	-1.8	-3.16	-2.81	-2.74	-3.01	-3.24
	VDW	-3.96	-4.83	-4.91	-4.78	-5.16	-7.31
	RMSD	2.33	2.71	2.64	2.55	0.48	2.55
	H-bond	1	3	1	1	4	2
	Binding Domain	TBD	CBD	CBD	TBD	GBD‡‡	TBD

*Free Binding Energy; **Van Der Waals; ***Root-Mean-Square Deviation; †Hydrogen bond (H-bond); ††Colchicine Binding Domain; ‡Taxol Binding Domain ‡‡GTP Binding Domain

Table 1: Molecular docking of the compounds in the interaction with β-tubulin.

energy score (FBE = -4.37 Kcal) was obtained for CCL361R, which also showed the lowest root mean square deviation (RMSD) amongst all the ligands. Notably, the values of VDW interactions were significantly correlated with the FBE of the compounds. Of all the ligands analyzed, the VDW interaction value for CCL361R was the highest (Table 1). The aromatic interaction of residue F272 of β-tubulin with CCL360R in the model with the best energy score was analyzed (Figure 6B). We observed that the number of hydrogen bonds was not significantly correlated with free energy scores. Hydrogen bonds with low energy scores were observed for residue N258 with CCL360S, residues L275 and P274 with CCL361R, and residue D26 with CCL361S (Figure 6B).

The interactions between β-tubulin and the different ligands on a molecular surface colored based on hydrophobicity are shown in Figure 7A. The hydrophobic surface plays an essential role in the ligand-protein interactions by affecting the non-bonding contributions to binding energies. The M-loop and T7-loop surfaces show higher hydrophobicities at the exact ligand-binding areas, as indicated in Figure 7A. Analyses investigating the binding of ligands to the electrostatic surface of β-tubulin indicate that, although the surface of β-tubulin mostly exhibited a positive charge, TBD and CBD exhibited low charge values (Figure 7B).

FUCCI analyses of HeLa cells and Vero cells treated with

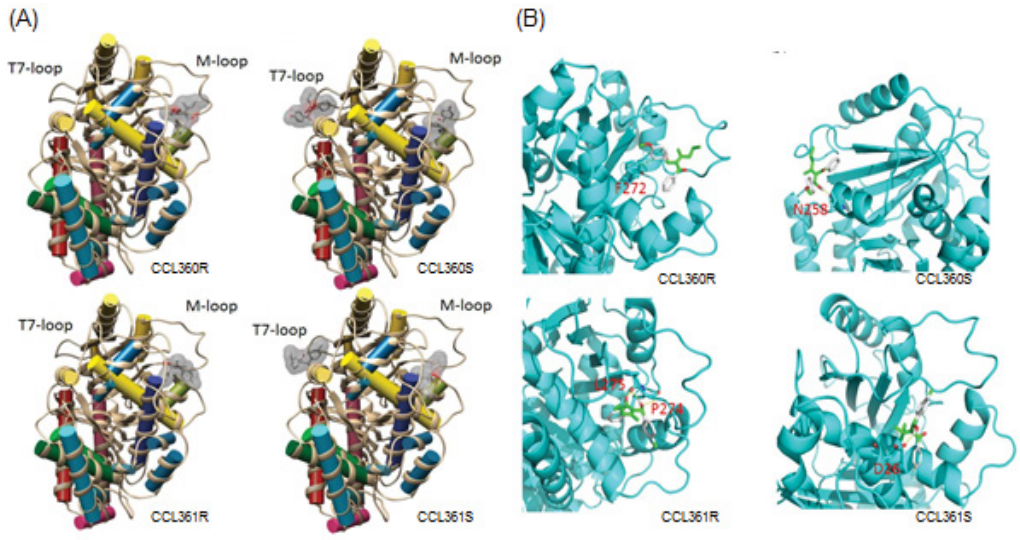

Figure 6: Docking analyses of the interactions between CCL360 and CCL361 with β-tubulin. (A) Atomic geometries of ligand-bound β-tubulin with the binding energy level of -3 Kcal or less for CCL360R, CCL360S, CCL361R, and CCL361S. (B) Magnified images of the atomic geometries of ligand-bound β-tubulin with lowest binding energy for CCL360R, CCL360S, CCL361R, and CCL361S.

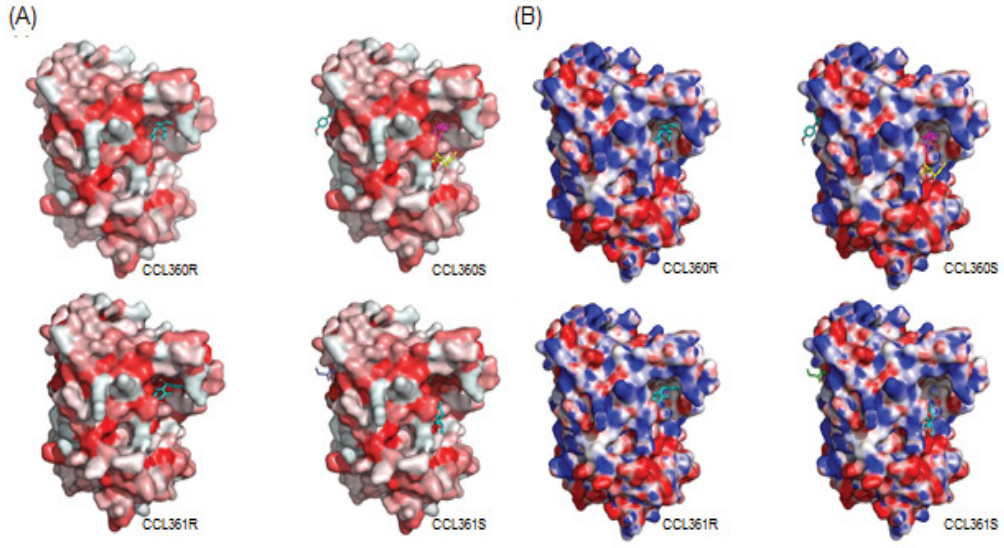

Figure 7: Interaction of CCL360 and CCL361 with β-tubulin. (A) Interactions of CCL360R, CCL360S, CCL361R, and CCL361S with the hydrophobic surfaces of β-tubulin (color-coded for hydrophobic (white) or hydrophilic (pink) at binding energy levels of -3 Kcal or less. (B) Interactions of CCL360R, CCL360S, CCL361R, and CCL361S with the electrostatic potential surface of β-tubulin (red: negative, blue: positive) with binding energy levels of -3 Kcal or less.

CCL360 and CCL361

The fluorescent ubiquitination-based cell cycle indicator (FUCCI) system was used to visualize the cell cycle behavior of individual cells treated with CCL360 and CCL361. FUCCI enabled us to determine the cell-cycle phase of individual cells by labeling G_1 nuclei red, and $S/G_2/M$ nuclei green. During the G_1/S transition, red and green fluorescence overlap, this was observed as yellow nuclei.

Time-lapse analyses of drug-treated HeLa-FUCCI cells for 24 h (Figure 8A) revealed that 37% of cells treated with CCL360 (Figure 8B) and 40% of cells treated with CCL361 (Figure 8C) showed a significantly prolonged M phase ($P < 0.001$, Welch's t-test) followed by cell division. We also observed that 25% of CCL360-treated cells remained arrested in the M phase and that 27% of these exhibited a prolonged M phase followed by apoptosis (Figure 8B); 38% of cells treated with CCL361, however, exhibited a prolonged M phase followed by apoptosis (Figure 8C). Prolonged G_1 phase or S/G_2 phase followed by apoptosis was observed in 13% and 9% of CCL361-treated cells, respectively (data not shown); however, this did not occur in CCL360-treated cells. Furthermore, Vero-FUCCI cells treated with CCL360 or CCL361 exhibited significantly prolonged S/G_2 and M phases ($P < 0.001$, Welch's t-test) as compared to DMSO-treated cells (Figures 8D and 8E).

Effects of CCL360 and CCL361 on the expression of cell cycle regulators

To examine the effects of CCL360 and CCL361 on the expression of G_2/M phase-associated cell cycle regulators, we conducted western blot analyses on the protein lysates of HeLa and Vero cells exposed to these two compounds (Figure 9). The expression levels of p53 and p21 in both HeLa and Vero cells were elevated after CCL360 and CCL361 treatments. To examine the effects of p53 and p21 induction on apoptosis, we also examined the levels of PARP fragments in these cells. Remarkably high levels of PARP cleavage were observed in HeLa cells after treatment with CCL360 and CCL361 for 24 h, suggesting that these compounds induced apoptosis in HeLa cells. Although some PARP cleavage was also detected in CCL360/61-treated Vero cells, levels were markedly lower than those observed in HeLa cells exposed to these two compounds.

Following these analyses, we also examined alterations in the levels of G_2/M regulatory proteins. An increase in the levels of p-histone H3 (at Ser10), which is phosphorylated during mitosis [35], was observed in drug-treated HeLa and Vero cells, indicating an increase in the population of cells in the M phase.

As shown in Figure 8, slight increases in cyclin B1 levels were also observed in both cell lines after treatment with CCL360 and CCL361. Since cyclin B/Cdc2 activation is essential for driving mitotic events [14], it may interrupt and suspend the process of mitotic exit (which is triggered by the degradation of Cyclin B at the metaphase) at the mitotic checkpoint [20]. Our results suggest that CCL360 and CCL361 likely induce mitotic arrest during prometaphase at the mitotic checkpoint.

Increases in the levels of phosphorylated Plk1 and dephosphorylated Cdc2 (at Tyr15) were observed in drug-treated HeLa cells, but not in Vero cells. Dephosphorylation of the Tyr15 residue of Cdc2 leads to the activation of Cdc2 at the G_2/M transition [36], which is mediated by Cdc25C, which is in turn activated by Plk1 [11,16,37]. Since p53 usually inhibits Plk1 [38], the simultaneous induction of p53 and Plk1 in drug-treated HeLa cells suggests a compromised link between p53 and Plk1 in these cells.

Discussion

In this study, we showed that the chalcone analogs CCL360 and CCL361 induced cell cycle arrest in the M phase followed by apoptosis in HeLa cells. Although these compounds prolonged the G_2/M phase in noncancerous Vero cells, they did not induce apoptosis.

The cytotoxicity assays and fluorescent ubiquitination-based cell

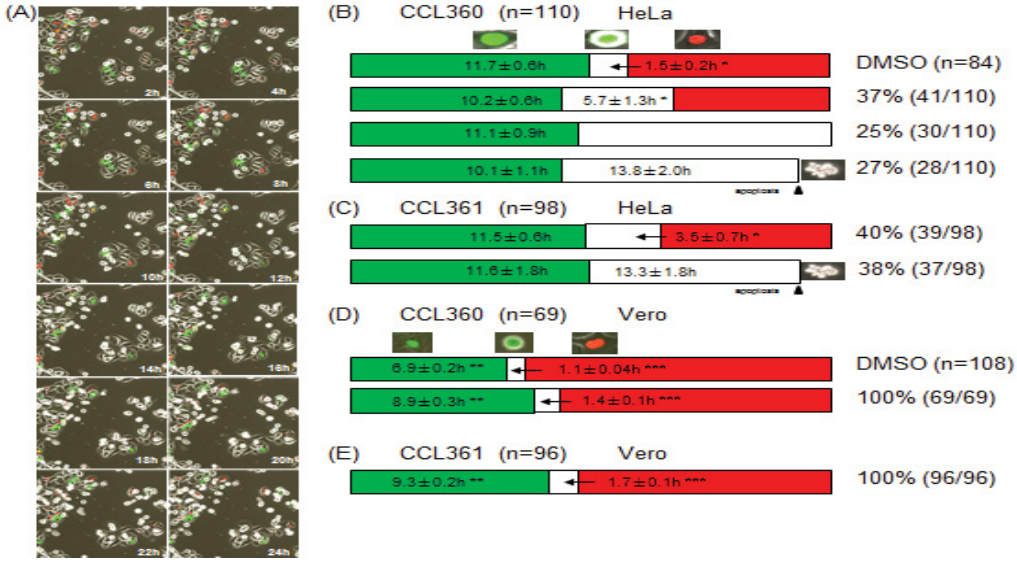

Figure 8: FUCCI analyses of HeLa and Vero cells treated with CCL360 and CCL361. Representative images of HeLa-FUCCI cells treated with CCL360 for 24 h (A). HeLa-FUCCI and Vero-FUCCI cells were exposed to 50 μM CCL360 (B and D) and CCL361 (C and E). Images of cells were obtained at 30-min intervals with a computer-assisted fluorescence microscope. The nuclei of HeLa-FUCCI and Vero-FUCCI cells fluoresced red during the G_1 phase and green during the $S/G_2/M$ phases. The mean periods of S/G_2 phases and M phases are shown as solid green and open bars, respectively; solid red bars represent the G_1 phase. Arrowheads indicate the time point of apoptosis. The mean periods are presented with standard errors. *$P < 0.001$, **$P < 0.001$, ***$P < 0.001$.

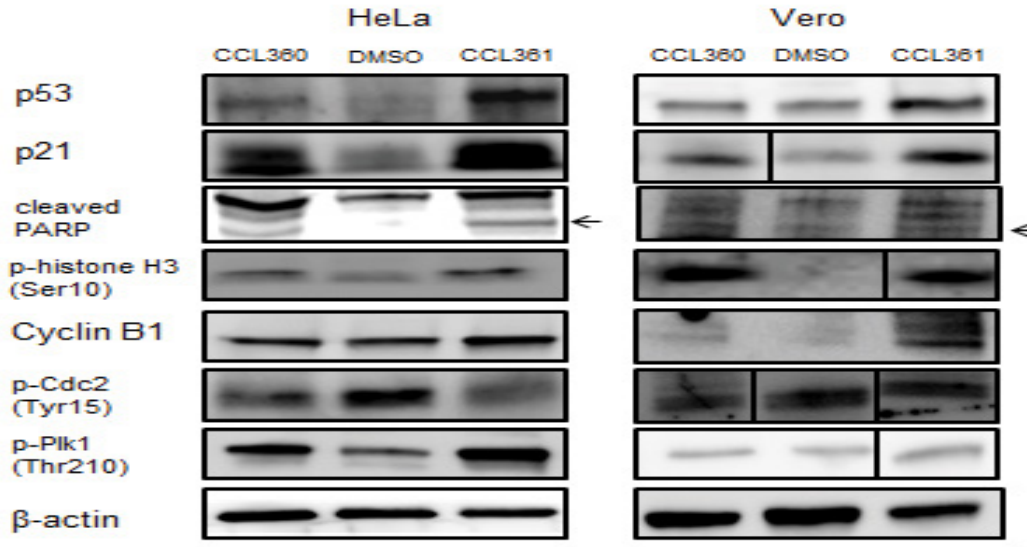

Figure 9: Western blot analyses of cell cycle regulating proteins from HeLa and Vero cells treated with CCL360 and CCL361. Total proteins from cells treated with 50 μM CCL360 or CCL361 for 24 h were subjected to western blot analyses for p53, p21, poly (ADP-ribose) polymerase (PARP), p-histone H3 (at Ser10), Cyclin B1, p-Plk1, and p-Cdc2 (at Tyr15). The arrows indicate the positions of indicated proteins. β-actin was used as an internal marker to show equivalent protein loading.

cycle indicator (FUCCI) analyses suggested that CCL361 was a more powerful antiproliferative agent than CCL360; this was consistent with the results of our docking study, where the binding energy of CCL361 to β-tubulin was lower than that of CCL360. Chalcones and their derivatives that inhibit tubulin assembly generally bind to β-tubulin at the colchicine binding domain (CBD) [21]; however, our docking studies suggest that the chalcone analogs CCL360 and CCL361 bind to β-tubulin via the taxol binding domain (TBD). Microtubule-targeting agents (MTAs) are usually classified based on their mechanism of action: microtubule stabilizers such as taxol and microtubule destabilizers such as the vinca alkaloids and colchicine [3,39]. Since CCL360 and CCL361 seem to bind to the TBD of β-tubulin, these two compounds are likely microtubule stabilizers, although most other chalcones usually function as microtubule destabilizers by binding to the CBD.

Treatment with CCL360/361 prolonged the G_2 phase in Vero cells, a phenomenon that was not observed in HeLa cells. It is likely that in the non-cancerous Vero cells treated with CCL360/61, the impairment in microtubule dynamics was detected at the cell cycle checkpoints; this, in turn, led to prolonged G_2/M phases for repair to occur. In HeLa cells, however, these checkpoints were possibly compromised, due to which CCL360/61-treated cells could not be repaired. These CCL360/61-treated HeLa cells probably entered the M phase with improperly formed microtubule structures and were stalled at the mitotic checkpoint, following which they died by apoptosis.

Activation of p53 and induction of p21 are involved in the cell cycle arrest induced by G_2/M checkpoint [11]. The increased levels of p53 and p21 in CCL360/361-treated HeLa and Vero cells highlight the similarities in the mechanism of action exhibited by these two compounds to that of taxol; taxol has been shown to induce the activation of p53 and accumulation of p21 independently of p53 [40].

Although the precise mechanisms by which CCL360 and CCL361 cause apoptosis specifically in HeLa cells, and not in Vero cells remain to be elucidated, one remarkable difference in cellular response between these two cell lines stands out was the activation of Plk1 in CCL360/361-treated HeLa cells, which does not occur in Vero cells. The activation of Plk1 is necessary for cells to enter the M phase, as this step is responsible for the activation of cyclin B1 and Cdc2 [11]. Furthermore, since activation of Plk1 is down-regulated by p53 as part of the G_2/M checkpoint [38], our results indicate that in HeLa cells, the link between Plk1 and p53 might be compromised and that this may partly be responsible for the selective toxicity of CCL360 and CCL361 to HeLa cells.

Conclusion

In conclusion, we report that the novel chalcone analogs CCL360 and CCL361, identified from the Chiba Chemical Library, show great potential as anticancer agents. Our study suggested that CCL360 and CCL361 may function like taxol. The two compounds can be used as lead compounds for developing new anticancer drugs.

Conflict of Interest

No conflicts of interest were disclosed.

References

1. Nussbaumer S, Bonnabry P, Veuthey JL, Fleury-Souverain S (2011) Analysis of anti-cancer drugs: A review. Talanta 85: 2265-2289.
2. Dumontet C, Jordan MA (2010) Microtubule-binding agents: A dynamic field of cancer therapeutics. Nature Reviews. Drug Discovery 9: 790-803.
3. Li L, Jiang S, Li X, Liu Y, Su J, et al. (2018) Recent advances in trimethoxyphenyl (TMP) based tubulin inhibitors targeting the colchicine binding site. European Journal of Medicinal Chemistry 151: 482-494.
4. Perez EA (2009) Microtubule inhibitors: Differentiating tubulin-inhibiting agents based on mechanisms of action, clinical activity, and resistance. Molecular Cancer Therapeutics 8: 2086-2095.
5. Risinger AL, Giles FJ, Mooberry SL (2009) Microtubule dynamics as a target in oncology. Cancer Treatment Reviews 35: 255-261.
6. Bates D, Eastman A (2017) Microtubule destabilising agents: far more than just antimitotic anticancer drugs. British Journal of Clinical Pharmacology 83: 255-268.

7. Negi AS, Gautam Y, Alam S, Chanda D, Luqman S, et al. (2015) Natural antitubulin agents: Importance of 3,4,5-trimethoxyphenyl fragment. Bioorganic & Medicinal Chemistry 23: 373-389.

8. Bhalla KN (2003) Microtubule-targeted anticancer agents and apoptosis. Oncogene 22: 9075-9086.

9. Jordan MA, Wilson L (2004) Microtubules as a target for anticancer drugs. Nature Reviews Cancer 4: 253-265.

10. Rohena CC, Mooberry SL (2014) Recent progress with microtubule stabilizers: new compounds, binding modes and cellular activities. Natural Product Reports 31: 335-355.

11. Zitouni S, Nabais C, Jana SC, Guerrero A, Bettencourt-Dias M (2014) Polo-like kinases: structural variations lead to multiple functions. Nature Publishing Group 15: 433-452.

12. Gavet O, Pines J (2010) Activation of cyclin B1-Cdk1 synchronizes events in the nucleus and the cytoplasm at mitosis. The Journal of Cell Biology 189: 247-259.

13. Jackman M, Lindon C, Nigg EA, Pines J (2003) Active cyclin B1-Cdk1 first appears on centrosomes in prophase. Nature Cell Biology 5: 143-148.

14. Neri L, Lasa M, Elosegui-Artola A, D'Avola D, Carte B, et al. (2017) NatB-mediated protein N-alpha-terminal acetylation is a potential therapeutic target in hepatocellular carcinoma. Oncotarget 8: 40967-40981.

15. Takizawa CG, Morgan DO (2000) Control of mitosis by changes in the subcellular location of cyclin-B1-Cdk1 and Cdc25C. Curr Opin Cell Biol 12: 658-665.

16. Cogswell JP, Brown CE, Bisi JE, Neill SD (2000) Dominant-negative polo-like kinase 1 induces mitotic catastrophe independent of cdc25C function. Cell Growth & Differentiation 11: 615-623.

17. Lindqvist A, Rodríguez-Bravo V, Medema RH (2009) The decision to enter mitosis: feedback and redundancy in the mitotic entry network. The Journal of Cell Biology 185: 193-202.

18. Toyoshima-Morimoto F, Taniguchi E, Nishida E (2002) Plk1 promotes nuclear translocation of human Cdc25C during prophase. Embo Reports 3: 341-348.

19. Hayashi MT, Karlseder J (2013) DNA damage associated with mitosis and cytokinesis failure. Oncogene 32: 4593-4601.

20. Musacchio A (2015) The molecular biology of spindle assembly checkpoint signaling dynamics. Current Biology : CB 25: R1002-R1018.

21. Mirzaei H, Emami S (2016) Recent advances of cytotoxic chalconoids targeting tubulin polymerization: Synthesis and biological activity. European Journal of Medicinal Chemistry 121: 610-639.

22. Dimmock JR, Elias DW, Beazely MA, Kandepu NM (1999) Bioactivities of chalcones. Current Medicinal Chemistry 6: 1125-1149.

23. Yasumura Y, Kawakita Y (1963) A line of cells derived from African green monkey kidney. Nippon Rinsho 21: 1209-1210.

24. Yi R, Saito K, Isegawa N, Shirasawa H (2015) Alteration of cell cycle progression by Sindbis virus infection. Biochemical and Biophysical Research Communications 462: 426-432.

25. Kellogg EH, Hejab NMA, Howes S, Northcote P, Miller JH, et al. (2017) Insights into the distinct mechanisms of action of taxane and non-taxane microtubule stabilizers from cryo-EM structures. Journal of Molecular Biology 429: 633-646.

26. Hanwell MD, Curtis DE, Lonie DC, Vandermeersch T, Zurek E, et al. (2012) Avogadro: an advanced semantic chemical editor, visualization, and analysis platform. Journal of Cheminformatics 4: 17.

27. Becke AD (1998) Density-functional thermochemistry. III. The role of exact exchange. The Journal of Chemical Physics 98: 5648-5652.

28. Lee C, Yang W, Parr RG (1988) Development of the Colle-Salvetti correlation-energy formula into a functional of the electron density. Physical Review B 37: 785-789.

29. Morris GM, Huey R, Lindstrom W, Sanner MF, Belew RK, et al. (2009) AutoDock4 and AutoDockTools4: Automated docking with selective receptor flexibility. Journal of Computational Chemistry 30: 2785-2791.

30. Morris GM, Goodsell DS, Halliday RS, Huey R, Hart WE, et al. (1998) Automated docking using a Lamarckian genetic algorithm and an empirical binding free energy function. Journal of Computational Chemistry 19: 1639-1662.

31. Eisenberg D, Schwarz E, Komaromy M, Wall R (1984) Analysis of membrane and surface protein sequences with the hydrophobic moment plot. Journal of Molecular Biology 179: 125-142.

32. Baker NA, Sept D, Joseph S, Holst MJ, McCammon JA (2001) Electrostatics of nanosystems: Application to microtubules and the ribosome. Proceedings of the National Academy of Sciences of the United States of America 98: 10037-10041.

33. Pettersen EF, Goddard TD, Huang CC, Couch GS, Greenblatt DM, et al. (2004) UCSF Chimera--A visualization system for exploratory research and analysis. Journal of Computational Chemistry 25: 1605-1612.

34. Mahapatra DK, Bharti SK, Asati V (2015) Anti-cancer chalcones: Structural and molecular target perspectives. European Journal of Medicinal Chemistry 98: 69-114.

35. Crosio C, Fimia GM, Loury R, Kimura M, Okano Y, et al. (2002) Mitotic phosphorylation of histone H3: Spatio-temporal regulation by mammalian aurora kinases. Molecular and Cellular Biology 22: 874-885.

36. Smits VAJ, Essers MAG, Loomans DSE, Klompmaker R, Rijksen G, et al. (1999) Inhibition of cell proliferation by lithium is associated with interference in cdc2 activation. FEBS Letters 457: 23-27.

37. Hoffmann I, Clarke PR, Marcote MJ, Karsenti E, Draetta G (1993) Phosphorylation and Activation of Human Cdc25-C by Cdc2 Cyclin-B and Its Involvement in the Self-Amplification of Mpf at Mitosis. The EMBO Journal 12: 53-63.

38. McKenzie L, King S, Marcar L, Nicol S, Dias SS, et al. (2010) p53-dependent repression of polo-like kinase-1 (PLK1). Cell Cycle (Georgetown, Tex.) 9: 4200-4212.

39. Kumar N (1981) Taxol-induced polymerization of purified tubulin. Mechanism of action. The Journal of Biological Chemistry 256: 10435-10441.

40. Blagosklonny MV, Schulte TW, Nguyen P, Mimnaugh EG, Trepel J, et al. (1995) Taxol induction of p21WAF1 and p53 requires c-raf-1. Cancer Research 55: 4623-4626.